

Superconductivity in FeSe: the role of nematic order

Jian Kang,¹ Rafael M. Fernandes,² and Andrey Chubukov²

¹*National High Magnetic Field Laboratory, Florida State University, Tallahassee, Florida 32304 USA*

²*School of Physics and Astronomy, University of Minnesota, Minneapolis, MN 55455, USA*

Bulk FeSe is a special iron-based material in which superconductivity emerges inside a well-developed nematic phase. We present a microscopic model for this nematic superconducting state, which takes into account the mixing between s -wave and d -wave pairing channels and the changes in the orbital spectral weight promoted by the sign-changing nematic order parameter. We show that nematicity only weakly affects T_c , but gives rise to $\cos 2\theta$ variation of the pairing gap on the hole pocket, whose magnitude and size agrees with ARPES and STM data. We further show that nematicity increases the weight of d_{xz} orbital on the hole pocket, and increases (reduces) the weight of d_{xy} orbital on Y (X) electron pocket.

Introduction. Superconductivity in FeSe has attracted a lot of attention recently because this material holds the promise to reveal new physics not seen in other Fe-based superconductors [1]. The pairing in FeSe emerges at $T \leq 8$ K from a state with a well-defined nematic order, which develops at a much higher $T_s \sim 90$ K. Because nematic order breaks the C_4 tetragonal symmetry down to C_2 , it mixes the s -wave and d -wave pairing channels [2–4]. As a result, the pairing gap on the Γ -centered hole pocket, $\Delta(\theta)$, has both s -wave and d -wave components, $\Delta(\theta) = \Delta_1 + \Delta_2 \cos 2\theta$, where Δ_1 and Δ_2 are C_4 -symmetric functions of $\cos 4\theta$. This gap form is generic, but the relative sign between Δ_1 and Δ_2 depends on details of the pairing interaction and the structure of the nematic order.

The $\cos 2\theta$ gap anisotropy on the hole pocket (“ h ” pocket in Fig. 1) has been probed recently by angle resolved photoemission spectroscopy (ARPES) [5–9] and scanning tunneling microscopy (STM) [10, 11] measurements. These probes have shown that (i) The gap is larger along the direction towards the X electron pocket made out of d_{yz} and d_{xy} orbitals, than towards the Y pocket made out of d_{xz} and d_{xy} orbitals (Fig. 1); and (ii) The magnitude of the gap on the X pocket correlates with the weight of the d_{yz} orbital component. This led to the proposal [10] that the pairing glue in FeSe is orbital-selective and predominantly involves fermions from the d_{yz} orbital.

To support this argument, Refs. [10, 12] analyzed the pairing problem within BCS theory, using the static interaction in the spin channel as the glue. They argued that the observed gap anisotropy can be reproduced only if one phenomenologically re-calibrates the interactions on d_{xz} , d_{yz} , and d_{xy} orbitals and set the interaction on the d_{yz} orbital to be the strongest. This was done by introducing phenomenologically different constant Z -factors for each orbital. A constant Z does not give rise to incoherence, but affects the magnitudes of the interactions on different orbitals.

In this paper we reconsider this issue. We argue that one has to distinguish the difference between d_{xy} orbital and d_{xz}/d_{yz} orbitals, and the difference between d_{xz} and d_{yz} orbitals. The dressed interactions on the d_{xy} orbital

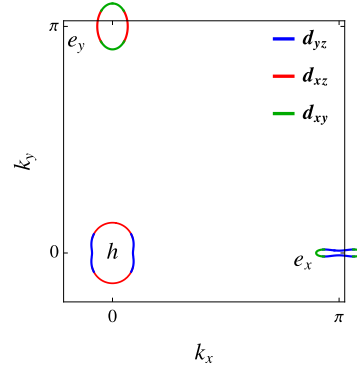


Figure 1. The Fermi surface and its orbital content in the nematic phase of FeSe. In the 1-Fe Brillouin zone there is a hole (h) pocket centered at $\Gamma/Z = (0, 0)$ and two electron pockets X and Y centered at $(\pi, 0)$ and $(0, \pi)$, respectively. STM and ARPES data [5, 10] show that the h pocket is an ellipse elongated along Y , and that the X electron pocket has a peanut-type form with the minor axis along the Y direction.

and on the d_{xz}/d_{yz} orbitals are not equal already in the tetragonal phase and flow to different values as one progressively integrates out contributions from high-energy fermions [13–15]. Adding different constant Z -factors to the d_{xy} and d_{xz}/d_{yz} orbitals is a legitimate way to incorporate these high-energy renormalizations into the low-energy model. On the other hand, the interactions on d_{xz} and d_{yz} orbitals become different only in the presence of nematic order. The latter is of order 10 meV (Refs. [10, 16, 17]), much smaller than the electronic bandwidth. As a result, the d_{xz}/d_{yz} splitting is a low-energy phenomenon which should be fully captured within the low-energy model, without introducing phenomenologically $Z_{xz} \neq Z_{yz}$.

In our approach we depart from the tetragonal phase with the Γ/Z -, X -, and Y -centered Fermi pockets in the 1-Fe Brillouin zone. We use the low-energy model of Ref. [18] to parametrize the dispersion near these three points, and the model of Ref. [13] for the d_{xz}/d_{yz} pairing interactions in the s -wave and d -wave channels. We introduce a two-component d -wave nematic order pa-

parameter $\bar{\Phi} = (n_{d_{xz}} - n_{d_{yz}})/2 = (\bar{\Phi}_h, \bar{\Phi}_e)$, where h and e refer to hole and electron pockets. It reconstructs the dispersion and the Fermi pockets to the ones shown in Fig. 1. ARPES and STM data [5–10, 16, 17, 19] reveal an ellipsoidal hole pocket elongated along the Y direction, and a peanut-like X electron pocket. A simple analysis shows that such Fermi surfaces emerge if $\Phi_h > 0$ and $\Phi_e < 0$, i.e. the nematic order changes sign between hole and electron pockets. This sign change is consistent with theoretical analysis [13, 20–22]. We take as an input the results of earlier studies [13–15, 20, 23, 24] that the largest pairing interaction at low-energies is between hole and electron pockets. This interaction is angle-dependent in the band basis and has s^{+-} and $d_{x^2-y^2}$ components U_s and U_d , respectively. U_s is larger, and in the absence of nematicity the system develops s^{+-} order, which changes sign between hole and electron pockets. We dress up U_s and U_d by coherence factors associated with the nematic order, solve the gap equation, and obtain T_c and the structure of the superconducting gap [25].

Our results show that T_c is only moderately affected by nematicity, but the nematic order gives rise to a sizable anisotropy of the gap on both hole and electron pockets. This is consistent with: (i) The phase diagram of S-doped $\text{FeSe}_{1-x}\text{S}_x$, which shows that T_c changes little around $x < 0.17$, when nematic order disappears; and (ii) Thermal conductivity, specific heat, and STM data [26–29], which show that the gap anisotropy changes drastically between $x < 0.17$ and $x > 0.17$.

For the gap on the hole pocket we find $\Delta(\theta_h) \approx \Delta_h(1 + \alpha \cos 2\theta_h + \beta \cos 4\theta_h)$, where the $\cos 2\theta_h$ term is induced by nematicity. To leading order in $\bar{\Phi}$, $\alpha \propto (4|\Phi_e| - (U_d/U_s)\Phi_h)$, where $\Phi_{h,e}$ are dimensionless orbital orders, normalized to the corresponding Fermi energies (see [30] and Eq (5) below). The Φ_h term reflects the nematicity-induced mixing between the s and d pairing components whereas the Φ_e term is related to the nematicity-induced redistribution of orbital weight on the electron pockets. The experimental angular dependence of the gap is reproduced when the Φ_e term is larger. We computed $\Phi_{h,e}$ using band structure parameters which fit the ARPES data for the Z pocket ($k_z = \pi$) [30] and found $|\Phi_e| \sim 0.1$, $\Phi_h \sim 0.3$. Combining this with the fact that $U_s \geq U_d$, we see that α is positive. A positive α can be interpreted as if nematicity makes the pairing interaction between the Γ and X pockets stronger than between the Γ and Y pockets. We emphasize that this effect is fully captured within the low-energy model.

In Fig. 2 we show the calculated $\Delta(\theta_h)$ along with the gap anisotropy extracted from the STM data [10]. We see that the agreement is quite good. We found equally good agreement with the ARPES data for the Z -pocket [5–8]. Whether STM is probing the Z ($k_z = \pi$) or the Γ pocket ($k_z = 0$) is difficult to determine, since STM data is likely averaged over k_z . We also computed the gap at the smaller Γ pocket ($k_z = 0$) and found a smaller gap with a weaker anisotropy. This arises because the dimensionless Φ_h is larger for smaller pockets and because,

unlike the Z pocket, the whole Γ pocket has predominantly d_{xz} character [30]. A smaller gap at Γ agrees with the ARPES data in [5, 7] but not with [9].

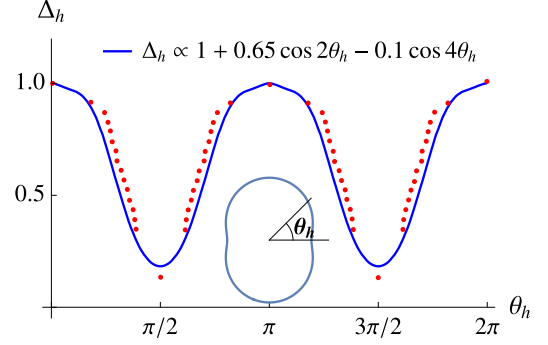


Figure 2. Angular dependence of the pairing gap on the hole pocket obtained by numerically solving the gap equations with band structure parameters and nematic order parameters fitted to ARPES data above T_c . The gap maximum is along the $\Gamma - X$ direction, consistent with STM and ARPES data [5–10, 19]. Points are STM data from Ref. [10]. The gap function $\Delta(\theta_h) = \Delta_h(1 + \alpha \cos 2\theta_h + \beta \cos 4\theta_h)$ has the $\cos 2\theta$ terms induced by nematicity (which we explicitly computed), as well as C_4 -symmetric anisotropic $\cos 4\theta$ terms present already in the tetragonal phase due to spin-orbit coupling [18] and/or due to dressing of the pairing interaction by high-energy fermions [13, 23].

Low-energy model. We consider a quasi-2D model of bulk FeSe, which in the tetragonal phase has two corrugated cylindrical hole pockets, centered at the $k_{x,y} = 0$ with the largest cross-section at $k_z = \pi$ and the smallest at $k_z = 0$ (Refs. [5, 7, 9, 16, 31]) and two cylindrical electron pockets centered at $(\pi, 0, k_z)$ and $(0, \pi, k_z)$ in the Fe-only Brillouin zone (X and Y pockets). The hole pockets are made out primarily of d_{xz} and d_{yz} orbitals, the X pocket is made primarily out of d_{yz} and d_{xy} orbitals, and the Y pocket, of d_{xz} and d_{xy} orbitals. We model the low-energy electronic structure on each pocket by spinors, following Ref. [18, 32]. We choose parameters such that the larger hole pocket h has d_{xz} character along the Y direction and d_{yz} character along the X direction, consistent with ARPES experiments [5–7, 9, 16, 19, 31].

The band operators for h , X , and Y pockets are expressed in terms of the orbital operators as

$$\begin{aligned} h &= d_{yz} \cos \phi_h + d_{xz} \sin \phi_h \\ e_X &= -id_{yz} \cos \phi_X + d_{xy} \sin \phi_X \\ e_Y &= id_{xz} \cos \phi_Y + d_{xy} \sin \phi_Y, \end{aligned} \quad (1)$$

In the tetragonal phase, the h -pocket is nearly circular and in the absence of spin-orbit coupling (SOC) $\phi_h \approx \theta_h$, where θ_h is the angle measured with respect to the X axis. On electron pockets, to a good approximation $\cos \phi_{X,Y} = A \sin \theta_{X,Y}$, $\sin \phi_{X,Y} = (1 - A^2 \sin^2 \theta_{X,Y})^{1/2}$, where $A < 1$ and θ_X (θ_Y) is the angle measured with respect to the X (Y) direction [3, 14].

In the nematic phase we introduce momentum-dependent d -wave nematic order with components $\pm\bar{\Phi}_h$ (plus sign on d_{xz} orbital) and $\bar{\Phi}(Y) = -\bar{\Phi}(X) = \bar{\Phi}_e$. For simplicity we neglect the d_{xy} component of the nematic order [14, 33]. Eqs. (1) still hold in the presence of nematicity, but the relations between ϕ_h, ϕ_X, ϕ_Y and the angles along the Fermi surfaces become different and are obtained by the diagonalization of the corresponding quadratic Hamiltonians. For the hole pocket, we define the dimensionless Φ_h via $\cot 2\phi_h = \cot 2\theta_h - 2\Phi_h / \sin 2\theta_h$, again in the absence of SOC (the full expressions including SOC are presented in [30]). Roughly, $\Phi_h = \bar{\Phi}_h / E_F$. For the same $\bar{\Phi}_h$, Φ_h is larger on the Γ pocket than on Z pocket, because E_F is smaller in the former.

For the electron pockets we find that the relations $\cos \phi_{X,Y} = A \sin \theta_{X,Y}$ also hold, but A becomes different for X and Y pockets. We define the dimensionless Φ_e via $A_X \approx A(1 - \Phi_e)$ and $A_Y \approx A(1 + \Phi_e)$, up to $O(\Phi_e^2)$ terms. To match ARPES and STM data for the shapes of the h and X pockets, Φ_h must be positive and Φ_e negative. A positive Φ_h increases the d_{xz} spectral weight on the hole pocket, particularly when $\Phi_h > 1/2$, see Fig. 3a. At $\Phi_e \sim 1$ the hole pocket is almost entirely d_{xz} . A negative Φ_e increases the weight of the d_{yz} orbital on the X pocket and reduces the weight of the d_{xz} orbital on the Y pocket, as shown in Fig. 3b. We computed the dimensionless $\Phi_{h,e}$ using $\bar{\Phi}_h = 10\text{meV}$, $|\bar{\Phi}_e| \sim 20\text{meV}$ (Refs. [10, 17, 34]) and band structure parameters that fit the ARPES data for the Z pocket [34, 35] in the nematic phase above T_c and obtained [30] $|\Phi_e| \sim 0.1$, $\Phi_h \sim 0.3$. For such Φ_h the orbital weight along the Z pocket still interpolates between d_{xz} and d_{yz} and does not depend strongly on the SOC. To simplify our analysis we then neglect SOC in the solution of the gap equations.

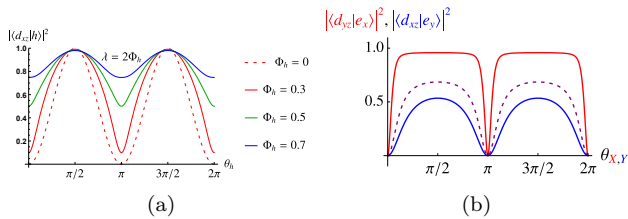


Figure 3. The change of orbital weight on the hole pocket (a) and on the electron pockets (b) between the tetragonal phase (dashed line) and the nematic phase (solid lines). The angle θ_X (θ_Y) is measured with respect to the X (Y) direction. For the hole pocket, we present the results including the SOC $\bar{\lambda}$ (the band splitting at $k_{x,y} = 0$ is $\pm\sqrt{\bar{\Phi}^2 + \bar{\lambda}^2/4}$). We used $\bar{\lambda} = 2\bar{\Phi}_h$.

Pairing interaction. The pairing interaction has three components – one involves fermions near the hole pocket, another involves fermions near the two electron pockets, and the third one is the pair hopping between hole and electron pockets. At the bare level all three interactions are comparable, but the pair-hopping term gets enhanced once one integrates out fermions with high

energies [10, 13–15, 23]. This enhancement can be understood as an indication of the system’s tendency to increase magnetic fluctuations at momenta connecting the Γ/Z and the X,Y points, consistent with the neutron scattering data [36–38]. We therefore consider only the pair hopping term for the pairing problem. In the band basis, the pair-hopping pairing interaction has the form

$$H_{\text{pair}} = h_k^\dagger h_{-k}^\dagger [U_s (e_{X,p} e_{X,-p} \cos^2 \phi_X + e_{Y,p} e_{Y,-p} \cos^2 \phi_Y) + U_d \cos 2\phi_h (e_{X,p} e_{X,-p} \cos^2 \phi_X - e_{Y,p} e_{Y,-p} \cos^2 \phi_Y)] \quad (2)$$

where repeated momentum indices are implicitly summed and spin indices are omitted. In the tetragonal phase, $\cos^2 \phi_{X,Y} = A^2(1 - \cos 2\theta_{X,Y})/2$, $\phi_h = \theta_h$, and the two terms in (2) describe pairing interactions in the s -wave and d -wave channels with couplings U_s and U_d , respectively. The ratio $U_s/U_d = (U + J)/(U - J) > 1$ already at the bare level, where U and J are Hubbard and Hund’s interactions, and further increases under RG [13]. Then the leading instability in the absence of nematicity is towards s^{+-} superconductivity.

In the presence of nematic order the situation changes because now $\cos 2\phi_h \approx \cos 2\theta_h - \Phi_h$ and $A_X \neq A_Y$. As a result, the U_d term in (2) acquires extra terms which have an “ s -wave” angular dependence and effectively renormalize the U_s term, making this interaction different for fermions near the X and Y pockets. Substituting the forms of $\cos 2\phi_h, \cos 2\phi_X$ and $\cos 2\phi_Y$ into (2) and restricting to first-order terms in Φ_h and Φ_e , we obtain the pairing interaction in the form

$$H_{\text{pair}} = \frac{A^2}{2} \sum_{j=X,Y} h_k^\dagger h_{-k}^\dagger (A_j + B_j \cos 2\theta_h) e_{j,p} e_{j,-p} \quad (3)$$

where

$$\begin{aligned} A_{X,Y} &= (1 - \cos 2\theta_{X,Y}) [U_s (1 \mp 2\Phi_e) \mp U_d \Phi_h] \\ B_{X,Y} &= \pm U_d (1 - \cos 2\theta_{X,Y}) (1 \mp 2\Phi_e) \end{aligned} \quad (4)$$

Gap equations. We use Eqs. (3) and (4) to obtain the linearized gap equations. The gap on the hole pocket is parametrized by $\Delta(\theta_h) = \Delta_h(1 + \alpha \cos 2\theta_h)$, (we neglect $\cos 4\theta$ term to simplify presentation). The computational steps are rather conventional [30]. To linear order in $\Phi_{e,h}$,

$$\alpha \approx \frac{U_s U_d}{U_s^2 - U_d^2/2} \left(4|\Phi_e| - \frac{U_d}{U_s} \Phi_h \right) \quad (5)$$

Notice that α depends only on the ratio U_d/U_s , and not on the strength of the interaction, which is compensated by the Cooper logarithm.

We see that there are two contributions to the gap anisotropy α , originating from the components of the nematic order on hole and electron pockets. Because Φ_h and Φ_e have opposite signs, the sign of α depends on their strength and on the ratio between the interactions

U_d/U_s . Because $4|\Phi_e| > \Phi_h$ and $U_d/U_s \leq 1$, we find $\alpha \sim 0.2$ is positive, i.e., the gap $\Delta_h(\theta_h)$ has its maximum along the X direction $\theta_h = 0$. This is consistent with the STM and ARPES data [5–10, 19]. The Φ_h term in (5) is further reduced if we take into account the fact that the ratio U_s/U_d grows under the renormalization group flow [13].

To go beyond this analytic expansion in powers of $\Phi_{e,h}$, we solved the gap equations numerically for the same set of parameters, but not restricting to first order in $\Phi_{h,e}$. We found the same gap structure but somewhat larger $\alpha \approx 0.65$. The result is shown in Fig. 2 along with the STM data from Ref. [10]. For this plot, we added to $\Delta(\theta_h)$ additional $\beta \cos 4\theta_h$ term with $\beta = -0.1$. The $\cos 4\theta_h$ dependence arises already in the tetragonal phase and is determined by details beyond our model.

The sign of the gap anisotropy can be interpreted as the indication that in the nematic state the pairing interaction between the h and X pockets becomes stronger than between the h and Y pockets. Because the positive contribution to α comes from Φ_e , the increase of the $h - X$ interaction can be traced back to the increase of d_{yz} orbital weight on the X pocket. In this respect, qualitatively our results agree with Refs. [10, 12], where the increase of the d_{yz} orbital weight was introduced phenomenologically, via an orbital dependent constant Z -factor. However, in our theory the modification of the d_{xz}/d_{yz} orbital weights naturally emerges within the low-energy model and does not require the inclusion of additional Z -factors.

On the electron pockets, to leading order in $\Phi_{h,e}$, the gaps have the forms $\Delta_{X,Y} = -\Delta_h \gamma_{X,Y} (1 - \cos 2\theta_{X,Y})$, where $\gamma_{X,Y} = \gamma [1 \pm (2|\Phi_e| - U_d/U_s \Phi_h + \alpha/2)]$ and $\gamma > 0$ is a number whose value depends on the electronic structure. The vanishing of the gaps at $\cos 2\theta_{X,Y} = \pm 1$ is an artifact of neglecting the d_{xy} orbital in the pairing problem. In reality, the gaps $\Delta_{X,Y}$ tend to small but finite values along the X and Y directions, respectively. The ARPES and STM data reported an anisotropic, but still sign-preserving gap on the X pocket, with gap maximum at $\theta_X = \pi/2$, consistent with our formulas. The overall sign of $\Delta_{X,Y}$ is opposite to that of Δ_h . The dependence of $\gamma_{X,Y}$ on the nematic order shows that the gap magnitude is larger on the X pocket than on the Y pocket. We propose to verify this in future experiments.

Fermionic self-energy. The STM data indicate that in the nematic phase the Y pocket is less visible than the X pocket, and in some ARPES studies [9, 39] this Y pocket has not been observed. To understand this feature, we computed the self-energy on both electron pockets to second order in U_s and U_d and extracted the actual quasiparticle residues $Z_{X,Y}$ on each electron pocket [30]. We find $Z_Y > Z_X$ simply because the effective interaction is larger for fermions on the X pocket (we recall that larger interaction leads to a smaller Z). If this was the only ef-

fect, we would expect the Y pocket to become more visible. However, like we said, nematic order also increases the d_{yz} spectral weight of the X pocket and decreases the d_{xz} orbital spectral weight of the Y pocket (see Fig. 3). If the d_{xy} orbital excitations are not observed in STM and ARPES because of matrix elements, or if the d_{xy} orbital is more incoherent than the d_{xz}/d_{yz} orbitals [40–43], then the Y pocket should indeed become less visible in the nematic phase. We caution, however, that recent ARPES study [9] did not find d_{xy} excitations on the X pockets to be more incoherent than d_{yz} excitations, so the reason why the Y pocket is less visible in STM and some ARPES studies is not yet understood.

Conclusions. In this paper we argued that the experimentally observed anisotropy of the superconducting gap in bulk FeSe can be explained within the low-energy model for nematic order, without adding phenomenologically different quasiparticle weights for the d_{xz}/d_{yz} orbitals. Our key result is that T_c is not strongly affected by the nematic order, but nematicity mixes s -wave and d -wave pairing channels and gives rise to a $\cos 2\theta_h$ gap anisotropy on the hole pocket. The sign of the $\cos 2\theta_h$ term is determined by the interplay between the nematic order parameters on hole and electron pockets, which are of different sign, and the relative strength of s -wave and d -wave components of the pairing interaction. On the Z pocket, we found a sizable $\cos 2\theta_h$ gap anisotropy with the gap maximum along the X direction, in agreement with the data. In our calculations the gap on the Γ pocket is smaller and less anisotropic. On the peanut-like X pocket, the gap is found to be maximal along the minor axis, which is also in agreement with the data. We also argued that nematicity decreases the weight of the d_{xy} orbital on the X pocket and increases it on the Y pocket. This may potentially explain why the Y pocket is less visible in STM and in some ARPES data.

ACKNOWLEDGMENTS

We are thankful to B. Andersen, L. Bascones, L. Benfatto, S. Borisenko, A. Coldea, M. Eschrig, P. Hirschfield, A. Kreisel, C. Meingast, L. Rhodes, J.C. Séamus Davis, O. Vafek, M. Watson, and Y. Y. Zhao for useful discussions. JK was supported by the National High Magnetic Field Laboratory through NSF Grant No. DMR-1157490 and the State of Florida. RMF and AVC were supported by the Office of Basic Energy Sciences, U.S. Department of Energy, under awards de-sc0012336 (RMF) and de-sc0014402 (AVC). J.K. thanks FTPI at the University of Minnesota for hospitality during the completion of this work. The authors are thankful to KITP at UCSB, where part of the work has been done. KITP is supported by NSF grant PHY 17-48958.

-
- [1] see e.g., A. Böhmer and A. Kreisel, *Journal of Physics: Condensed Matter* **30**, 023001 (2017) and references therein.
- [2] R. M. Fernandes, and A. J. Millis, *Phys. Rev. Lett.* **111**, 127001 (2013);
- [3] J. Kang, A. F. Kemper, and R. M. Fernandes, *Phys. Rev. Lett.* **113**, 217001 (2014).
- [4] G. Livanas, A. Aperis, P. Kotetes, and G. Varelogiannis, *Phys. Rev. B* **91**, 104502 (2015).
- [5] H. C. Xu, X. Niu, D. F. Xu, J. Jiang, Q. Yao, Q. Y. Chen, Q. Song, M. Abdel-Hafiez, D. A. Chareev, A. N. Vasiliev, Q. S. Wang, H. L. Wo, J. Zhao, R. Peng, and D. L. Feng, *Phys. Rev. Lett.* **117**, 157003 (2016).
- [6] T. Hashimoto, Y. Ota, H. Q. Yamamoto, Y. Suzuki, T. Shimojima, S. Watanabe, C. Chen, S. Kasahara, Y. Matsuda, T. Shibauchi, K. Okazaki, and S. Shin, *Nat. Comm.* **9**, 282 (2018).
- [7] Y. S. Kushnirenko, A. V. Fedorov, E. Haubold, S. Thirupathaiah, T. Wolf, S. Aswartham, I. Morozov, T. K. Kim, B. Büchner, and S. V. Borisenko, *arXiv:1802.08668*.
- [8] D. Liu, C. Li, J. Huang, B. Lei, L. Wang, X. Wu, B. Shen, Q. Gao, Y. Zhang, X. Liu, Y. Hu, Y. Xu, A. Liang, J. Liu, P. Ai, L. Zhao, S. He, Li Yu, G. Liu, Y. Mao, X. Dong, X. Jia, F. Zhang, S. Zhang, F. Yang, Z. Wang, Q. Peng, Y. Shi, J. Hu, T. Xiang, X. Chen, Z. Xu, C. Chen, and X. J. Zhou, *arXiv:1802.02940*. The authors measure the gap on the Γ pocket, but the size of their pocket is larger than in other ARPES studies and is consistent with what other groups found for the Z-pocket.
- [9] L. C. Rhodes, M. D. Watson, A. A. Haghighirad, D. V. Evtushinsky, M. Eschrig, and T. K. Kim, *arXiv:1804.01436*.
- [10] P. O. Sprau, A. Kostin, A. Kreisel, A. E. Böhmer, V. Taufour, P. C. Canfield, S. Mukherjee, P. J. Hirschfeld, B. M. Andersen, and J. C. Séamus Davis, *Science* **357**, 6346 (2017); see also A. Kostin, P. O. Sprau, A. Kreisel, Y.-X. Chong, A. E. Böhmer, P. C. Canfield, P. J. Hirschfeld, B. M. Andersen, and J.C. Séamus Davis, *arXiv:1802.02266*.
- [11] L. Jiao, C.-L. Huang, S. Rößler, C. Koz, U. K. Rößler, U. Schwarz, and S. Wirth, *Scientific Reports*, **7**, 44024 (2017).
- [12] A. Kreisel, B. M. Andersen, P. O. Sprau, A. Kostin, J.C. Séamus Davis, P. J. Hirschfeld, *Phys. Rev. B* **95**, 174504 (2017).
- [13] A. V. Chubukov, M. Khodas, R. M. Fernandes, *Phys. Rev. X* **6**, 041045 (2016).
- [14] R.-Q. Xing, L. Classen, M. Khodas, A. V. Chubukov, *Phys. Rev. B* **95**, 085108 (2017); L. Classen, R.-Q. Xing, M. Khodas, A. V. Chubukov, *Phys. Rev. Lett.* **118**, 037001 (2017).
- [15] Fa Wang, H. Zhai, Y. Ran, A. Vishwanath, and Dung-Hai Lee, *Physical Review Letters*, **102**, 047005 (2009); C. Platt, W. Hanke, and R. Thomale, *Advances in Physics* **62**, 453-562 (2013).
- [16] A. I. Coldea and M. D. Watson, *Annual Review of Condensed Matter Physics*, **9**, 125 (2018).
- [17] A. Fedorov, A. Yaresko, T. K. Kim, Y. Kushnirenko, E. Haubold, T. Wolf, M. Hoesch, A. Grüneis, B. Büchner, and S. V. Borisenko, *Scientific Reports*, **6**, 36834 (2016).
- [18] V. Cvetkovic and O. Vafek, *Phys. Rev. B* **88**, 134510 (2013).
- [19] Y. Suzuki, T. Shimojima, T. Sonobe, A. Nakamura, M. Sakano, H. Tsuji, J. Omachi, K. Yoshioka, M. Kuwata-Gonokami, T. Watashige, R. Kobayashi, S. Kasahara, T. Shibauchi, Y. Matsuda, Y. Yamakawa, H. Kontani, and K. Ishizaka, *Phys. Rev. B* **92**, 205117 (2015).
- [20] S. Onari, Y. Yamakawa, and H. Kontani, *Phys. Rev. Lett.* **116**, 227001 (2016).
- [21] L. Fanfarillo, J. Mansart, P. Toulemonde, H. Cercellier, P. Le Fevre, F. m. c. Bertran, B. Valenzuela, L. Benfatto, and V. Brouet, *Phys. Rev. B* **94**, 155138 (2016).
- [22] L. Benfatto, B. Valenzuela, L. Fanfarillo, *arXiv:1804.05800*.
- [23] S. Graser, T. A. Maier, P. J. Hirschfeld, and D. J. Scalapino, *New J. Phys.* **11**, 025016 (2009).
- [24] A.V. Chubukov, *Annul. Rev. Cond. Mat. Phys.* **3**, 13.1 (2012).
- [25] We did not set the pairing interaction to be different for d_{xz} and d_{yz} orbitals due to nematic order. Such renormalization is rather weak if one introduces orbital order and directly compute the splitting of interactions on d_{xz} and d_{yz} orbitals [10, 43]. The situation may be different if nematicity is due to composite Ising spin order [22].
- [26] P. Bourgeois-Hope, S. Chi, D. A. Bonn, R. Liang, W. N. Hardy, T. Wolf, C. Meingast, N. Doiron-Leyraud, and L. Taillefer, *Phys. Rev. Lett.* **117**, 097003 (2016).
- [27] L. Wang, F. Hardy, T. Wolf, P. Adelman, R. Fromknecht, P. Schweiss, C. Meingast, *Phys. Status Solidi B* **254**, 1600153 (2017).
- [28] Y. Sato, S. Kasahara, T. Taniguchi, X.Z. Xing, Y. Kasahara, Y. Tokiwa, T. Shibauchi, and Y. Matsuda, *arXiv:1705.09074*.
- [29] T. Hanaguri, K. Iwaya, Y. Kohsaka, T. Machida, T. Watashige, S. Kasahara, T. Shibauchi, and Y. Matsuda, *arXiv:1710.02276*.
- [30] see Supplementary Material.
- [31] M. D. Watson, T. K. Kim, A. A. Haghighirad, N. R. Davies, A. McCollam, A. Narayanan, S. F. Blake, Y. L. Chen, S. Ghannadzadeh, A. J. Schofield, M. Hoesch, C. Meingast, T. Wolf, and A. I. Coldea, *Phys. Rev. B* **91**, 155106 (2015).
- [32] R. M. Fernandes and A. V. Chubukov, *Rep. Prog. Phys.* **80**, 014503 (2017).
- [33] R. M. Fernandes and O. Vafek, *Phys. Rev. B* **90**, 214514 (2014).
- [34] M. D. Watson, T. K. Kim, L. C. Rhodes, M. Eschrig, M. Hoesch, A. A. Haghighirad, and A. I. Coldea, *Phys. Rev. B* **94**, 201107 (2016).
- [35] A. I. Coldea, private communication.
- [36] M. C. Rahn, R. A. Ewings, S. J. Sedlmaier, S. J. Clarke, and A. T. Boothroyd, *Phys. Rev. B* **91**, 180501 (2015).
- [37] Q. Wang, Y. Shen, B. Pan, Y. Hao, M. Ma, F. Zhou, P. Steffens, K. Schmalzl, T. R. Forrest, M. Abdel-Hafiez, X. Chen, D. A. Chareev, A. N. Vasiliev, P. Bourges, Y. Sidis, H. Cao, and J. Zhao, *Nat. Mater.* **15**, 159 (2016).
- [38] Q. Wang, Y. Shen, B. Pan, X. Zhang, K. Ikeuchi, K. Iida, A. D. Christianson, H. C. Walker, D. T. Adroja, M. Abdel-Hafiez, X. Chen, D. A. Chareev, A. N. Vasiliev, and J. Zhao, *Nat. Comm.* **7**, 12182 (2016).
- [39] M. D. Watson, A. A. Haghighirad, L. C. Rhodes, M. Hoesch, T. K. Kim, *New J. Phys.* **19**, 103021 (2017)

- [40] N. Lanata, H. U. R. Strand, G. Giovannetti, B. Hellsing, L. de Medici, and M. Capone, Phys. Rev. B **87**, 045122 (2013).
 [41] Z. P. Yin, K. Haule, and G. Kotliar, Nat. Mater. **10**, 932 (2011).
 [42] E. Bascones, B. Valenzuela, and M. J. Calderón, Phys. Rev. B **86**, 174508 (2012).
 [43] L. Fanfarillo, G. Giovannetti, M. Capone, and E. Bascones, Phys. Rev. B **95**, 144511 (2017).

Supplementary material for “Anisotropic superconductivity in FeSe without orbital selectivity”

I. DETAILS OF THE LOW-ENERGY MODEL

A. Hole Pockets

The dispersion near the hole pockets centered at $k_{x,y}$ is expressed in terms of the two-component spinor $\psi_\Gamma = (d_{xz}, d_{yz})^T$. We follow Refs. [18, 32] and write the Hamiltonian in the tetragonal phase in the absence of spin-orbit coupling (SOC) as

$$H_h^{(0)} = \psi_h^\dagger \left(\left(\epsilon_h - \frac{k^2}{2m_h} \right) \tau_0 - \frac{b}{2} (k_x^2 - k_y^2) \tau_3 - 2ck_x k_y \tau_1 \right) \psi_h = \psi_h^\dagger (H_0 \tau_0 - \frac{b}{2} k^2 \cos 2\theta_h \tau_3 - ck^2 \sin 2\theta_h \tau_1) \psi_h, \quad (\text{S1})$$

where θ_h is the angle measured with respect to the X axis (we work in the 1-Fe Brillouin zone). The free parameters of this Hamiltonian are shown in Table S1, and are obtained from fitting to ARPES data on the Z -pocket ($k_z = \pi$) [34, 35]. All the energy parameters are in units of meV, and the momentum are in units of the inverse lattice constant.

ϵ_h	$(2m_h)^{-1}$	b	c
13.6	473	529	-265

Table S1. Band parameters of the hole pocket.

The dispersion for the two hole pockets can easily be obtained numerically. It is also instructive to obtain an approximate analytical solution. For this purpose, note that the parameters in the Table give $b \approx -2c > 0$. In this case, the band dispersions around Z can be approximated as

$$H_h^{(0)} \approx H_0(k) \tau_0 + H_1(k) (-\cos 2\theta_h \tau_3 + \sin 2\theta_h \tau_1) \quad (\text{S2})$$

with $H_0 = \epsilon_h - k^2/(2m_h)$ and $H_1(\mathbf{k}) \approx bk^2/2$. Diagonalization leads to Eq. (1) of the main text with $\varphi_h = \theta_h$ and an isotropic dispersion, $\epsilon_{1,2}^Z = \epsilon_h - k^2/(2m_h) \pm bk^2/2$. We will be mostly interested in the larger hole pocket. Its dispersion is given by $\epsilon_1^Z = \epsilon_h - k^2(1/(2m_h) - b/2)$.

In the nematic phase, the Hamiltonian acquires the extra term $H_{h(\text{nem})} = \bar{\Phi}_h \psi_h^\dagger \tau_3 \psi_h$ (see Ref. [33]). The total Hamiltonian $H_h = H_h^{(0)} + H_{h(\text{nem})}$ is then:

$$H_h \approx H_0(k) \tau_0 + ((\bar{\Phi}_h - H_1 \cos 2\theta_h) \tau_3 + H_1 \sin 2\theta_h \tau_1) \longrightarrow H_0(k) \tau_0 + H_1' (-\cos 2\varphi_h \tau_3 + \sin 2\varphi_h \tau_1) \quad (\text{S3})$$

with $(0 \leq \theta_h \leq \pi/2)$

$$\cot 2\varphi_h \approx \frac{H_1 \cos 2\theta_h - \bar{\Phi}_h}{H_1 \sin 2\theta_h} = \cot 2\theta_h - \frac{\bar{\Phi}_h}{H_1 \sin 2\theta_h} \implies \varphi_h \approx \theta_h + \Phi_h \sin 2\theta_h \quad (\text{S4})$$

where we defined the dimensionless nematic order parameter $\Phi_h \equiv \bar{\Phi}_h/2H_1(k_F)$, where $H_1(k_F) = bk_F^2/2$. Using the numbers from the Table, we estimate on the Z pocket $2H_1(k_F) \approx 30$ meV and $\bar{\Phi}_h \approx 10$ meV. This yields $\Phi_h \approx 0.3$.

On the Γ pocket, k_F is smaller [5, 7, 9, 39], and for the same $\bar{\Phi}_h$, the dimensionless Φ_h is larger, at least by a factor of 2.

In addition to the change in the orbital composition of the Γ pocket, nematicity also deforms the shape of Fermi surface. The change in the dispersion is $\delta\epsilon_h = -\bar{\Phi}_h \cos 2\theta_h$, giving rise to a change in the Fermi momentum $\delta k_F \sim -\bar{\Phi}_h \cos 2\theta_h/v_f$. Consequently, the Fermi pocket changes shape from circular to elliptical. When $\bar{\Phi}_h$ is positive, its major axis points along Y direction, while the minor axis points along X direction.

1. Orbital content of the hole pocket

In the tetragonal phase the weight of the d_{xz} component along the larger hole pocket is $\sin^2 \theta_h$ and the weight of d_{yz} component is $\cos^2 \theta_h$. Along the X direction, the orbital content is entirely d_{yz} , and along the Y direction it is entirely d_{xz} . In the nematic phase, the weight of d_{xz} is $\sin^2 \varphi_h$ and the weight of d_{yz} is $\cos^2 \varphi_h$. Eq. (S4) can be re-expressed as

$$\cot 2\varphi_h \approx \frac{\cos 2\theta_h - 2\Phi_h}{\sin 2\theta_h} \quad (\text{S5})$$

An elementary analysis shows that the orbital weight at $\theta_h = 0$ (i.e., along the X direction) now depends on whether $2\Phi_h < 1$ or $2\Phi_h > 1$. For smaller Φ_h , $\varphi_h(\theta_h = 0) = 0$, i.e., the weight along X is entirely d_{yz} . At $\theta_h = \pi/2$, $\varphi_h = \pi/2$, i.e., along Y , the orbital composition is d_{xz} , as in the absence of the nematicity. At arbitrary θ_h , φ_h is different from θ_h , and the orbital content changes compared to the one in the tetragonal phase. We show the weight of d_{xz} along the hole pocket in Fig. S1a. It increases in the nematic phase but still vanishes at $\theta_h = 0, \pi$.

The situation changes when $\Phi_h > 1/2$. From Eq. (S5) we now have $\varphi_h(\theta_h = 0) = \pi/2$, i.e., the weight along X is now entirely d_{xz} . At $\theta_h = \pi/2$, we still have $\varphi_h = \pi/2$, i.e., the orbital weight is entirely d_{xz} . This is a non-trivial change of orbital composition of the hole pocket in the tetragonal phase. In Fig. S2 we show the orbital content of d_{xz} along the larger hole pocket at various Φ_h . We see that along the X direction it jumps from 0 to 1 between $\Phi_h < 1/2$ and $\Phi_h > 1/2$.

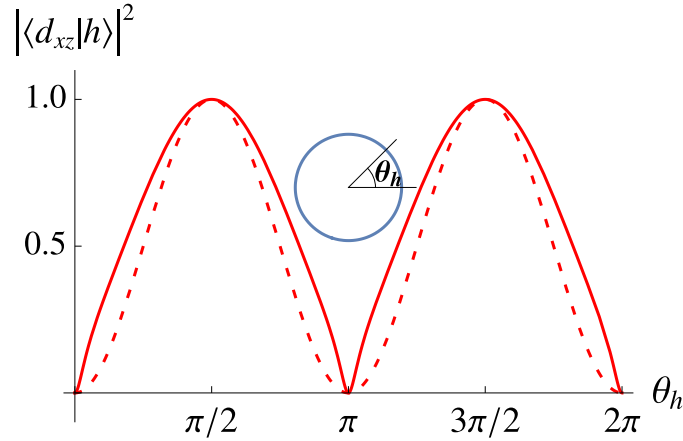


Figure S1. The change of orbital weight on the hole pocket between the tetragonal phase (dashed line) and the nematic phase (solid lines) in the absence of SOC. The angle is measured with respect to the X direction.

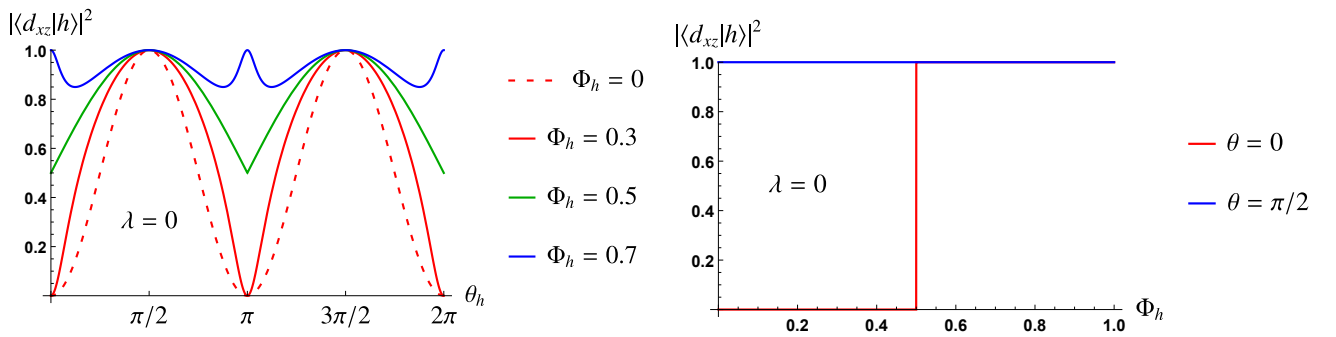


Figure S2. (a) The change of orbital weight on the hole pocket between the tetragonal phase (dashed line) and the nematic phase (solid lines) for different Φ_h in the absence of SOC. The angle is measured with respect to the X direction. (b) The d_{xz} orbital weight at $\theta_h = 0$ and $\theta_h = \pi/2$ as a function of Φ_h .

We now add SOC. It gives rise to additional term in the quadratic form [18]

$$H_{h,SOC} = \frac{\bar{\lambda}}{2} \psi_{h,\alpha}^\dagger \tau_2 \psi_{h,\beta} \sigma_{\alpha\beta}^3 \quad (S6)$$

where α, β are spin indices, and τ_2 acts on orbital indices. At $k_{x,y} = 0$, the splitting between the larger and smaller hole pockets is now $2\sqrt{\bar{\Phi}_h^2 + \bar{\lambda}^2/4}$. One can easily check that in the presence of SOC the dispersions of the two hole pockets repel each other and do not cross along any direction (at $\lambda = 0$ they necessary cross at some momentum). Because of no-crossing, the smaller hole pocket sinks completely below the Fermi level when $\sqrt{\bar{\Phi}_h^2 + \bar{\lambda}^2/4} > \epsilon_h$.

Re-diagonalizing the quadratic form, we now obtain on a larger hole Fermi surface, instead of (S5)

$$\cot 2\varphi_h \approx \frac{\cos 2\theta_h - 2\Phi_h}{\sqrt{\sin^2 2\theta_h + \lambda^2}} \quad (S7)$$

where $\lambda = \bar{\lambda}/H_1(k_F)$ is the dimensionless SOC constant. One can easily verify that now the orbital content along both X and Y directions is neither d_{xz} nor d_{yz} , although along Y it remains quite close to pure d_{xz} for realistic $\lambda \sim \Phi_h$. We show the orbital weight of d_{xz} along the hole pocket for several Φ_h and $\lambda = 2\Phi_h$ in Fig. 3a of the main text. Here we show, in Fig.S3 the evolution of the spectral weight of d_{xz} with λ for several Φ_h . In Fig. S4 we show the evolution of the d_{xz} weight at $\theta_h = 0$ and $\theta_h = \pi/2$ as a function of Φ_h for $\lambda = 2\Phi_h$. Note the rapid increase of the spectral weight of d_{xz} at $\theta_h = 0$ around $\Phi_h = 1/2$ and weak dependence on Φ_h of the d_{xz} weight at $\theta_h = \pi/2$. On the Z pocket ($\Phi_h \sim 0.3$) the d_{xz} weight at $\theta_h = 0$ is rather small. However, if Φ_h on the Z pocket is a bit larger, the weight increase towards 50%. At $\Phi_h \sim 0.7 - 0.8$, expected for the Γ pocket, the weight of d_{xz} at $\theta_h = 0$ is around 80%. This agrees with the polarization ARPES analysis in [9].

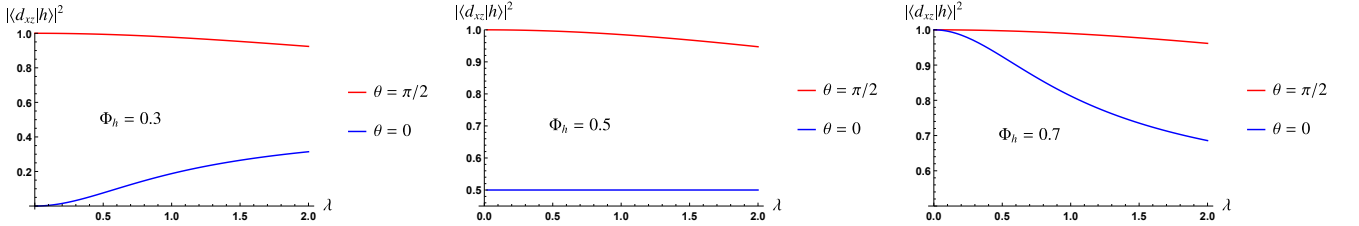


Figure S3. The evolution of the d_{xz} orbital weight on the hole pocket with increasing λ at three different Φ_h taken at and around critical $\Phi_h = 1/2$.

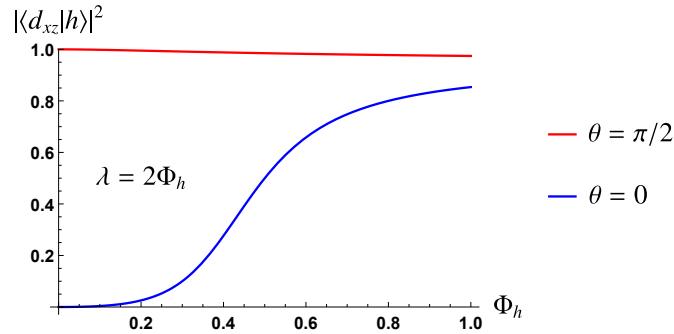


Figure S4. The evolution of the d_{xz} orbital weight on the hole pocket at $\theta_h = 0$ and $\theta_h = \pi/2$ with increasing Φ_h and $\lambda = 2\Phi_h$.

B. Electron Pockets

For the electron pockets, an analytic expression similar to the case of the hole pocket is not available. We start from the Hamiltonian [18, 32],

$$H_{X,Y} = \Psi_{X,Y}^\dagger \begin{pmatrix} \epsilon_1 + \frac{\mathbf{k}^2}{2m_1} \mp \frac{a_1}{2}(k_x^2 - k_y^2) & -iv_{X,Y}(\mathbf{k}) \\ iv_{X,Y}(\mathbf{k}) & \epsilon_3 + \frac{\mathbf{k}^2}{2m_3} \mp \frac{a_3}{2}(k_x^2 - k_y^2) \end{pmatrix} \Psi_{X,Y} \quad (\text{S8})$$

$$v_X(\mathbf{k}) = \sqrt{2}vk_y + \frac{p_1}{\sqrt{2}}(k_y^3 + 3k_yk_x^2) - \frac{p_2}{\sqrt{2}}k_y(k_x^2 - k_y^2), \quad v_Y(\mathbf{k}) = \sqrt{2}vk_x + \frac{p_1}{\sqrt{2}}(k_x^3 + 3k_xk_y^2) + \frac{p_2}{\sqrt{2}}k_x(k_x^2 - k_y^2)$$

Here we list the band parameters fitted to ARPES experiments [34, 35]. All the energy parameters are in units of meV, and the momenta are in units of the inverse lattice constant.

ϵ_1	ϵ_3	$(2m_1)^{-1}$	$(2m_3)^{-1}$	a_1	a_3	v	p_1	p_2
-19.9	-39.4	1.4	186	136	-403	-122	-137	-11.7

Table S2. Band parameters for the electron pockets.

Diagonalizing the Hamiltonian numerically, we found that the orbital composition of the X electron pocket can be fitted using the approximate form for the band operator in terms of the orbital operators:

$$e_X = -iA \sin \theta_X d_{yz} + \sqrt{1 - A^2 \sin^2 \theta_X} d_{xy} \quad (\text{S9})$$

The value of A can be estimated using the band parameters presented below, yielding $A^2 \approx 0.7$. Note that there is another band at the X pocket that does not cross the Fermi level. The corresponding operator, denoted here by \tilde{e}_X , is parametrized according to:

$$\tilde{e}_X = i\sqrt{1 - A^2 \sin^2 \theta_X} d_{yz} + A \sin \theta_X d_{xy} \quad (\text{S10})$$

An important quantity for our analysis is the energy splitting ΔE between these two bands calculated at k_F of the electron pocket. Using the ARPES fitted parameters, we find $\Delta E \sim 60\text{meV}$ for $\theta = \pi/2$.

Nematic order is included via:

$$H_{X,Y}^{(\text{nem})} = \mp \Delta_e^{(\text{nem})} \Psi_{X,Y}^\dagger \begin{pmatrix} 1 & 0 \\ 0 & 0 \end{pmatrix} \Psi_{X,Y}. \quad (\text{S11})$$

To leading order of $\Delta_e^{(\text{nem})}$, the wave function of the upper band becomes

$$e'_X \approx e_X + \frac{\Delta_e^{(\text{nem})}}{\Delta E} A \sin \theta_X \sqrt{1 - A^2 \sin^2 \theta_X} \left(i\sqrt{1 - A^2 \sin^2 \theta_X} d_{yz} + A \sin \theta_X d_{xy} \right) \quad (\text{S12})$$

At $\theta_X = \pi/2$, where the spectral weight of d_{yz} orbital is maximum, we find that e'_X can be expressed in the same form of e_X but with $A \rightarrow A_X = A + \delta A$, where:

$$\frac{\delta A}{A} \approx -\frac{\Delta_e^{(\text{nem})}}{\Delta E} (1 - A^2) \equiv -\Phi_e \quad (\text{S13})$$

Here, we defined the dimensionless nematic order parameter Φ_e . Using the values of A and ΔE mentioned above, and $\Delta_e^{(\text{nem})} \approx -18\text{meV}$, as indicated by ARPES measurements [16, 17], we find $\Phi_e \approx -0.1$.

II. PAIRING INTERACTION

As explained in the main text, the RG analysis allows us to focus only on two types of inter-pocket pairing interaction: the intra-orbital pairing U and inter-orbital pairing J . We find

$$H_{\text{pair}}^{(X)} = 2 \sum_{\mathbf{k}, \mathbf{p}} h_{\mathbf{k}\uparrow}^\dagger h_{-\mathbf{k}\downarrow}^\dagger (1 - t \cos 4\phi_h) (U \cos^2 \phi_h + J \sin^2 \phi_h) e_{X-\mathbf{p}\downarrow} e_{X\mathbf{p}\uparrow} \cos^2 \phi_X + h.c. \quad (\text{S14})$$

$$H_{\text{pair}}^{(Y)} = 2 \sum_{\mathbf{k}, \mathbf{p}} h_{\mathbf{k}\uparrow}^\dagger h_{-\mathbf{k}\downarrow}^\dagger (1 - t \cos 4\phi_h) (U \sin^2 \phi_h + J \cos^2 \phi_h) e_{Y-\mathbf{p}\downarrow} e_{Y\mathbf{p}\uparrow} \cos^2 \phi_Y + h.c. \quad (\text{S15})$$

Instead of deriving how the angular dependence of the hole gap arises due to SOC or renormalization, we introduce a phenomenological parameter $-t \cos 4\theta_h$ in the pairing interaction to account for the angular dependence of the SC gap on h even in the tetragonal phase. Note that the C_4 symmetry is still conserved in the presence of this term. In our numerical calculation, we set $t = 0.2 \ll 1$.

Adding them together yields:

$$H_{\text{pair}} = \sum_{\mathbf{k}, \mathbf{p}} h_{\mathbf{k}\uparrow}^\dagger h_{-\mathbf{k}\downarrow}^\dagger (1 - t \cos 4\phi_h) [U_s (e_{X,-\mathbf{p}\downarrow} e_{X,\mathbf{p}\uparrow} \cos^2 \phi_X + e_{Y,-\mathbf{p}\downarrow} e_{Y,\mathbf{p}\uparrow} \cos^2 \phi_Y) + U_d \cos 2\phi_h (e_{X,-\mathbf{p}\downarrow} e_{X,\mathbf{p}\uparrow} \cos^2 \phi_X - e_{Y,-\mathbf{p}\downarrow} e_{Y,\mathbf{p}\uparrow} \cos^2 \phi_Y)] + h.c. \quad (\text{S16})$$

with $U_s = U + J$ and $U_d = U - J$. In our calculation, we set $U_d = U_s$. Note that $\cos^2 \phi_{X,Y}$ is the orbital weight of $d_{yz,xz}$ on the $e_{X,Y}$ band and $\cos^2 \phi_h$ ($\sin^2 \phi_h$) are the weights of d_{yz} (d_{xz}) orbitals on the hole band. These weights can be obtained by diagonalization of the matrix $H_{\Gamma,X,Y}$ with the nematic terms.

As shown in the previous sections, $\cos^2 \phi_{X,Y} \approx A_{X,Y}^2 \sin^2 \theta_{X,Y}$ with $A_{X,Y} \approx A(1 \mp \Phi_e)$ if only the first order of the nematic order parameter $\Phi_{h,e}$ is kept in the expansion. Additionally, $\cos 2\phi_h \approx \cos 2\theta_h + \Phi_h \cos 4\theta_h - \Phi_h$. For small nematicity and $t \ll 1$, the $\cos 4\theta_h$ terms can be neglected in the pairing interaction. This gives

$$H_{\text{pair}} = \frac{A^2}{2} \sum_{j=X,Y} h_{\mathbf{k}}^\dagger h_{-\mathbf{k}}^\dagger (1 - \cos 2\theta_j) (A_j + B_j \cos 2\theta_h) e_{j,\mathbf{p}} e_{j,-\mathbf{p}} \quad (\text{S17})$$

$$\text{with } A_{X,Y} = [U_s(1 \mp 2\Phi_e) \mp U_d\Phi_h], \text{ and } B_{X,Y} = [\pm U_d - 2\Phi_e U_d] \quad (\text{S18})$$

III. SOLUTION OF THE GAP EQUATIONS

Starting with the pairing interaction presented in Eq. S16, the linearized gap equation becomes (see Fig. S5)

$$\Delta_h(\mathbf{k}_h) = - (1 - \beta \cos 4\theta_h) \left[(U_s + U_d \cos 2\phi_h) \int \frac{d^2 k}{(2\pi)^2} \frac{\tanh(\beta \epsilon_{X,\mathbf{k}}/2)}{2\epsilon_{X,\mathbf{k}}} \cos^2 \phi_X \Delta_X + (U_s - U_d \cos 2\phi_h) \int \frac{d^2 k}{(2\pi)^2} \frac{\tanh(\beta \epsilon_{Y,\mathbf{k}}/2)}{2\epsilon_{Y,\mathbf{k}}} \cos^2 \phi_Y \Delta_Y \right] \quad (\text{S19})$$

$$\Delta_X(\mathbf{k}_X) = - \cos^2 \phi_X \int \frac{d^2 k}{(2\pi)^2} \frac{\tanh(\beta \epsilon_{h,\mathbf{k}}/2)}{2\epsilon_{h,\mathbf{k}}} (1 - \beta \cos 4\phi_h) (U_s + U_d \cos 2\phi_h) \Delta_{h,\mathbf{k}} \quad (\text{S20})$$

$$\Delta_Y(\mathbf{k}_Y) = - \cos^2 \phi_Y \int \frac{d^2 k}{(2\pi)^2} \frac{\tanh(\beta \epsilon_{h,\mathbf{k}}/2)}{2\epsilon_{h,\mathbf{k}}} (1 - \beta \cos 4\phi_h) (U_s - U_d \cos 2\phi_h) \Delta_{h,\mathbf{k}} \quad (\text{S21})$$

We numerically solved this equation using the band structure and interaction parameters discussed above and the results are presented in Fig. 2. We found that the gap on the hole pocket is roughly proportional to $1 + 0.65 \cos 2\theta_h - 0.1 \cos 4\theta_h$.

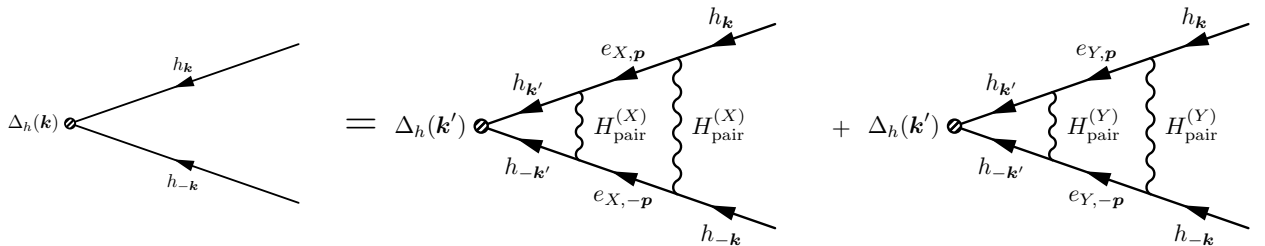


Figure S5. The gap equation for the hole pocket at $T = T_c$, with spin indices suppressed.

We proceed now with the derivation of the analytical expression of the SC gap in leading order in $\Phi_{h,e}$. For this

purpose, we start with the approximated pairing interaction in Eq. S17. The pairing equations become

$$\begin{aligned}
\Delta_h(\mathbf{k}_h) &= -A^2 \left[(A_X + B_X \cos 2\theta_h) \int \frac{d^2k}{(2\pi)^2} \frac{\tanh(\beta\epsilon_{X,\mathbf{k}}/2)}{2\epsilon_{X,\mathbf{k}}} \sin^2 \theta_X \Delta_X \right. \\
&\quad \left. + (A_Y + B_Y \cos 2\theta_h) \int \frac{d^2k}{(2\pi)^2} \frac{\tanh(\beta\epsilon_{Y,\mathbf{k}}/2)}{2\epsilon_{Y,\mathbf{k}}} \sin^2 \theta_Y \Delta_Y \right] \\
\Delta_X(\mathbf{k}_X) &= -A^2 \sin^2 \theta_X \int \frac{d^2k}{(2\pi)^2} \frac{\tanh(\beta\epsilon_{h,\mathbf{k}}/2)}{2\epsilon_{h,\mathbf{k}}} (A_X + B_X \cos 2\theta_h) \Delta_{h,\mathbf{k}} \\
\Delta_Y(\mathbf{k}_Y) &= -A^2 \sin^2 \theta_Y \int \frac{d^2k}{(2\pi)^2} \frac{\tanh(\beta\epsilon_{h,\mathbf{k}}/2)}{2\epsilon_{h,\mathbf{k}}} (A_Y + B_Y \cos 2\theta_h) \Delta_{h,\mathbf{k}}
\end{aligned} \tag{S22}$$

We can then parametrize the gaps as

$$\Delta_h = \Delta_1 + \Delta_2 \cos 2\theta_h, \quad \Delta_X = \Delta_3 \sin^2 \theta_X \text{ and } \Delta_Y = \Delta_4 \sin^2 \theta_Y. \tag{S23}$$

The gap equations for Δ_i can be written in a matrix form. To further simplify the notation, we define

$$\begin{aligned}
\Xi_X &= \int \frac{d^2k}{(2\pi)^2} \frac{\tanh(\beta\epsilon_{X,\mathbf{k}}/2)}{2\epsilon_{X,\mathbf{k}}} \sin^4 \theta_X & \Xi_Y &= \int \frac{d^2k}{(2\pi)^2} \frac{\tanh(\beta\epsilon_{Y,\mathbf{k}}/2)}{2\epsilon_{Y,\mathbf{k}}} \sin^4 \theta_Y \\
\Xi_{h,j} &= \int \frac{d^2k}{(2\pi)^2} \frac{\tanh(\beta\epsilon_{h,\mathbf{k}}/2)}{2\epsilon_{h,\mathbf{k}}} (\cos 2\theta_h)^j \quad \text{with } j = 0, 1, 2.
\end{aligned} \tag{S24}$$

All these integrals are $O(\ln(\Lambda/T))$, which is given by the band dispersion in the tetragonal phase. In the weak coupling limit, we therefore can keep only the logarithmic term to expand the SC gap to the leading order of nematicity and neglect the change of band dispersion by the nematicity. Therefore, $\epsilon_{e_X}(\theta) = \epsilon_{e_Y}$ and ϵ_h is still C_4 symmetric, leading to $\Xi_X = \Xi_Y = \Xi_e$ and $\Xi_{h,1} = 0$. Furthermore, with quadratic hole dispersion, $\Xi_{h,2} = \Xi_{h,0}/2$. $\Xi_{h,0} = \Pi_h$ is the usual particle-particle bubble for the hole pocket. The matrix equations for Δ_j becomes

$$\begin{pmatrix} \Delta_1 \\ \Delta_2 \end{pmatrix} = -A^2 \Xi_e \begin{pmatrix} A_X & A_Y \\ B_X & B_Y \end{pmatrix} \begin{pmatrix} \Delta_3 \\ \Delta_4 \end{pmatrix}, \quad \begin{pmatrix} \Delta_3 \\ \Delta_4 \end{pmatrix} = -A^2 \Pi_h \begin{pmatrix} A_X & B_X/2 \\ A_Y & B_Y/2 \end{pmatrix} \begin{pmatrix} \Delta_1 \\ \Delta_2 \end{pmatrix} \tag{S25}$$

To solve this equation, we write

$$\begin{pmatrix} \Delta_1 \\ \Delta_2 \end{pmatrix} = A^4 \Xi_e \Pi_h \begin{pmatrix} A_X & A_Y \\ B_X & B_Y \end{pmatrix} \begin{pmatrix} A_X & B_X/2 \\ A_Y & B_Y/2 \end{pmatrix} \begin{pmatrix} \Delta_1 \\ \Delta_2 \end{pmatrix} = (M_0 + M_1) \begin{pmatrix} \Delta_1 \\ \Delta_2 \end{pmatrix}, \tag{S26}$$

where the matrix M_0 contains no nematic terms, and $M_1 \sim O(\Phi_{h,e})$. With the expression of $A_{X,Y}$ and $B_{X,Y}$ in Eq. S18, we find

$$M_0 = 2A^4 \Xi_e \Pi_h \begin{pmatrix} U_s^2 & 0 \\ 0 & U_d^2/2 \end{pmatrix}, \quad M_1 = -A^4 \Xi_e \Pi_h (2U_d^2 \Phi_h + 8U_s U_d \Phi_e) \begin{pmatrix} 0 & 1/2 \\ 1 & 0 \end{pmatrix} \tag{S27}$$

We see Δ_1 and Δ_2 decouples in M_0 , reflecting that s - and d -wave are two pairing instabilities. When $U_s > U_d$, s -wave is the leading solution, with T_c given by the equation $2A^4 U_s^2 \Xi_e \Pi_h = 1$. s -wave and d -wave are mixed due to the perturbative term M_1 . To leading order in M_1 , the solution is given by

$$\alpha = \frac{\Delta_2}{\Delta_1} \approx -\frac{U_s U_d}{U_s^2 - U_d^2/2} \left(4\Phi_e + \frac{U_d}{U_s} \Phi_h \right). \tag{S28}$$

As we said before, we set $\Phi_e \sim -0.1$, $\Phi_h = 0.3$, and $U_d/U_s \leq 1$. This yields $\alpha \approx 0.2$. We recall that we used the dispersion for the Z-pocket ($k_z = \pi$). If we don't expand the gap to leading order in Φ_h and Φ_e and instead solve Eqs. S19–S21 numerically, we obtain larger $\lambda \sim 0.65$, which we cited in the main text. We present the result of the numerical solution in Fig. 2 of the main text. For completeness, we also present the result at the Γ point. Here Φ_h is larger and, hence, the gap anisotropy is smaller. We also found that the gap magnitude is reduced if we use the same values of U_s and U_d at Γ and at Z . We show the results in Fig. S6. A smaller gap at Γ is consistent with ARPES results in Refs. [5, 7]. The authors of [9], however, reported the gap at Γ larger than that at Z .

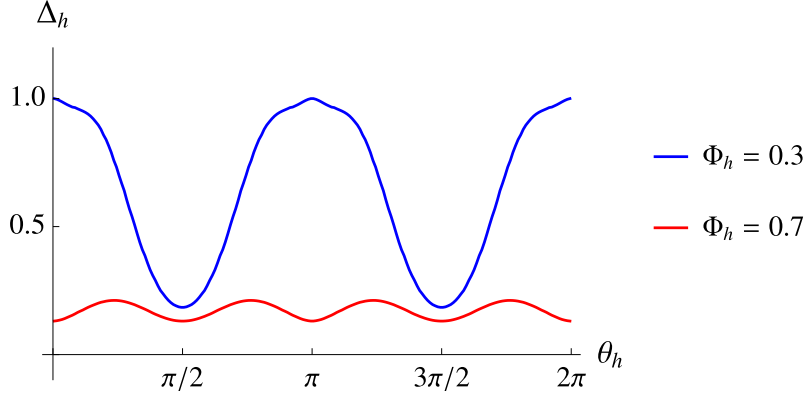


Figure S6. Superconducting gap on the Z pocket, in comparison with that on the Γ pocket (red). We used the same pairing interactions U_s and U_d at Γ and Z , same Φ_e and larger Φ_h at Γ than at Z .

For the electron pockets, we find:

$$\Delta_{e_X} = -A^2 \sin^2 \theta_X \Pi_h \left(A_X \Delta_1 + \frac{B_X}{2} \Delta_2 \right) \approx -A^2 \Pi_h \sin^2 \theta_X U_s \Delta_1 \left[1 - 2\Phi_e - \frac{U_d}{U_s} \left(\Phi_h - \frac{\alpha}{2} \right) \right] \quad (\text{S29})$$

$$\Delta_{e_Y} = -A^2 \sin^2 \theta_Y \Pi_h \left(A_Y \Delta_1 + \frac{B_Y}{2} \Delta_2 \right) \approx -A^2 \Pi_h \sin^2 \theta_Y U_s \Delta_1 \left[1 + 2\Phi_e + \frac{U_d}{U_s} \left(\Phi_h - \frac{\alpha}{2} \right) \right] \quad (\text{S30})$$

The vanishing of the gap at the edges of the pockets is the artefact of neglecting d_{xy} orbital. Once it is included, the gap remains highly anisotropic, but does not vanish anywhere on X (Y) pocket.